TURBULENCE MEASUREMENTS FROM 5-BEAM ACOUSTIC DOPPLER CURRENT PROFILERS

Maricarmen Guerra Paris* and Jim Thomson

Applied Physics Laboratory, University of Washington, Seattle, Washington

**Corresponding author address:* Maricarmen Guerra Paris, Applied Physics Laboratory, University of Washington, 1013 NE 40th Street, Box 355640, Seattle, WA 98105-6698.

E-mail: mguerrap@uw.edu

ABSTRACT

Two new 5-beam Acoustic Doppler Current Profilers, the Nortek Signature 1000 AD2CP and the Teledyne RDI Sentinel V50, are demonstrated to measure turbulence at two energetic tidal channels within Puget Sound, WA, USA. The quality of the raw data is tested by analyzing the turbulent kinetic frequency energy spectra, the turbulence spatial structure function, the shear in the profiles, and the covariance Reynolds stresses. The 5-beam configuration allows for a direct estimation of the Reynolds stresses from along-beam velocity fluctuations. The Nortek's low Doppler noise and high sampling frequency allow for the observation of the turbulent inertial subrange in both the frequency spectra and in the turbulence structure function. The obtained turbulence parameters from the 5-beam Acoustic Doppler Current Profilers are validated with turbulence data from simultaneous measurements with Acoustic Doppler Velocimeters. These combined results are then used to assess a turbulent kinetic energy budget, in which depth profiles of the turbulent kinetic energy dissipation and production rates are compared. The associated codes are publicly available on the Matlab File Exchange website.

1. Introduction

Acoustic Doppler Current Profilers (ADCPs) are commonly used to measure the horizontal components of fluid velocities along depth profiles in the ocean using three or four diverging acoustic beams. The raw data from ADCPs, termed pings, correspond to single velocity measurements in the along-beam direction. The raw ping data are typically burst-averaged in time (usually 5 -10 minutes in tidal flows, to ensure stationarity). Averaging reduces the Doppler noise inherent to the measurement, which can add significant variance to the raw signals (above and beyond the variance due to real turbulent fluctuations) (Brumley et al. 1991). However, if the raw along-beam velocities are retained, many turbulence parameters, such as turbulent kinetic energy dissipation rates and Reynolds stresses, can be estimated from ADCP measurements. Estimation methods are based on the variance and correlations of the along-beam velocity fluctuations, often with explicit removal of the variance contributed by the Doppler noise (Lu and Lueck 1999; Stacey et al. 1999; Wiles et al. 2006; Thomson et al. 2012).

Indirect methods to estimate turbulent dissipation rates, such as TKE spectra and the turbulence structure functions (Pope 2001), are based on Kolmogorov's theory of a turbulent cascade of eddies at smaller and smaller length scales, and require the observation of the inertial subrange of isotropic turbulence in the data (Pope 2001).

In the frequency domain, some authors (e.g Thomson et al. 2012; Richard et al. 2013; Durgesh et al. 2014) have attempted to use spectra calculated from raw along-beam velocity ADCP data, but the inherent Doppler noise typically obscures the inertial subrange (Richard et al. 2013). Recently, turbulence dissipation rates have been estimated from turbulence spectra after averaging the frequency spectra for different mean flows and bins in order to successfully observe the inertial subrange in the turbulence energy cascade in McMillan et al. (2016) and McMillan and Hay

(2017). Another common technique is to estimate turbulent dissipation rates using the second-order spatial structure function of turbulence (Wiles et al. 2006; Rusello and Cowen 2011).

One of the most frequently used techniques to estimate Reynolds stresses from ADCP along-beam velocities is the variance technique (Lu and Lueck 1999; Stacey et al. 1999; Rippeth et al. 2003), which provides two components (out of six) of the Reynolds stresses and is based on the variance of opposite beam velocity fluctuations.

A new generation of broadband 5-beam ADCPs with the ability to measure flow velocity at higher frequencies and with lower noise levels is poised to expand routine turbulence measurements. Moreover, the inclusion of a fifth beam allows for a true measurement of vertical velocities and the estimation of five (out of six) Reynolds stresses, total turbulent kinetic energy (TKE), and anisotropy directly from the along-beam velocities (Lu and Lueck 1999; Dewey and Stringer 2007). This is a notable expansion beyond the four-beam variance methods (Lu and Lueck 1999; Stacey et al. 1999; Rippeth et al. 2003).

This paper presents turbulence measurements from two new 5-beam acoustic current profilers: the Nortek Signature 1000 (kHz), which uses the acronym AD2CP to distinguish it from the previous generation of profilers, and the new Teledyne RDI Sentinel V50 500 (kHz). The new instruments' capabilities are assessed in two field deployments in highly energetic tidal channels, calculations of turbulence parameters, and the subsequent evaluation of turbulent kinetic energy (TKE) budgets.

The results are validated using measurements from Acoustic Doppler Velocimeters (ADVs), which are typically the preferred choice for turbulence measurements. However, ADVs only measure at a point, and their deployment at mid-depths requires complicated moorings and subsequent motion corrections to the raw data (Thomson et al. 2013). The new ADCPs are shown to be a more practical alternative to ADVs, with the potential for new insights about where turbulence is being produced and dissipated in the water column.

In Section 2 details of the field measurements are presented. In Section 3, estimates of the TKE dissipation rate are presented using two different methods: the TKE frequency spectra and the second-order spatial structure function. In Section 4, the terms of the TKE production rate are estimated; in particular, Reynolds stresses are calculated using along-beam velocities from all five beams. Finally, in Section 5, the TKE dissipation and production rate estimates are used to examine the TKE budget at the two tidal channels.

2. Data Collection

a. Site Description

Turbulence measurements were taken at Admiralty Inlet and Rich Passage, two tidal channels located in Puget Sound, WA, USA. Figure 1a shows the location of the field sites and the detailed locations of the instruments. A summary of the deployments and instrument settings is presented in Table 1.

Admiralty Inlet is located in the northern part of Puget Sound (48.14°N, 122.71° W). Admiralty Inlet is $\sim$ 6.5 km wide and $\sim$ 50 m deep at the measurement site. The principal direction of the flow is $\sim 50^\circ$ from the east in the clockwise direction.

Rich Passage is located south of Bainbridge island in Puget Sound (47.59° N, 122.56° W). At the measurements site the channel is $\sim$ 24 m deep and $\sim$ 550 m wide. The channel is oriented $\sim 45^\circ$ from north in the clockwise direction.

b. Instruments and Settings

The 5-beam Doppler profilers were deployed mounted looking upward on separate Oceanscience Sea Spider tripods, which place each instrument ~ 0.9 m above the seafloor when deployed. The instruments have four beams slanted at 25° from the vertical, plus a fifth vertical beam. Deployments were on May 11 2015 at Admiralty Inlet and on May 17 – 18 2015 at Rich Passage. Table 1 summarizes the deployments and sampling parameters.

The Nortek Signature was configured to measure turbulence in along-beam coordinates using its five beams at 8 Hz (the maximum possible when using all five beams) for ten minute bursts. At Admiralty Inlet, the burst interval was twenty minutes and there were 20 velocity bins at 1 m spacing. At Rich Passage, the burst interval was thirty minutes and there were 15 velocity bins at 1 m spacing.

The Teledyne RDI Sentinel V50, deployed at 48.1517°N, 122.6858°W, was configured to measure along-beam turbulent velocities at 2 Hz (the maximum possible when using all five beams) for 10 minute bursts with a 20 minute interval. At Admiralty Inlet, the RDI Sentinel V50 tripod was ~ 80 m away from the Nortek Signature tripod and there were 20 velocity bins at 1 m spacing. At Rich Passage, the Sentinel V50 was not deployed (it was unavailable).

In addition to the two 5-beam Acoustic Doppler Current Profilers, Acoustic Doppler Velocimeters (ADVs) were deployed at both sites in the vicinity of the instruments in order to compare and validate the data from the profilers.

At Admiralty Inlet, a Nortek Vector ADV was deployed 130 m east of the Nortek Signature on board a Tidal Turbulence Mooring (TTM) (Thomson et al. 2013; Harding et al. In revision; Kilcher et al. In revision) on May 11 – 13 2015. The TTM consists of an anchor (approx. 1000 kg wet weight) to hold the mooring in place, a sphere (approx. 300 kg positive buoyancy) to hold the mooring vertical, and an instrumentation vane inline between the anchor and the buoy where the ADV was mounted. The TTM positions the ADV at 10 m above the sea bottom. The ADV was set to measure velocities at 16 Hz continuously. An inertial motion unit (IMU) synchronously measured TTM acceleration and orientation; these data are used to remove contaminations of mooring motion from the ADV turbulent velocities. The motion correction method is described in detail in Thomson et al. (2013) and Kilcher et al. (In revision).

At Rich Passage, a Nortek Vector ADV was deployed in the same location as the Nortek Signature. The ADV was mounted on a Turbulence Torpedo (TT), a sounding weight that hangs from a davit on the side of the ship while the ship is holding station (Thomson et al. 2013; Harding et al. In revision; Kilcher et al. In revision). The Turbulence Torpedo ADV was deployed on June 5 2015, sampling turbulent velocities at 16 Hz for 2.5 hours during ebb tide (mean flow ranging between 1.5 and 2 m/s). Motion corrections were applied to the velocity measurements following the same methods used for the TTM ADV measurements (Thomson et al. 2013; Kilcher et al. In revision).

c. Raw Data

Figure 2 shows vertical profiles, and time series, of along channel velocity (after a coordinate transformation of the beam velocities) measured by the Nortek Signature for both study sites. At Admiralty Inlet, it was possible to measure only a single tidal cycle due to the rapid battery consumption when sampling at high frequency. After approximately 12 hours, the Nortek Signature kept sampling, but the bursts became shorter (less than the 10 minutes setting). At Rich Passage, a reduced duty cycle made it possible to measure two tidal cycles before the bursts became shorter. For both deployments, a single battery pack was used, but additional battery packs can be externally connected to the instrument to overcome the limits from rapid battery consumption.

The maximum observed burst-averaged horizontal speed at Admiralty Inlet was 2.04 m/s during flood which corresponds to a Reynolds number of $\mathscr{O}(10^8)$. At Rich Passage the maximum burst-averaged observed horizontal speed was 1.95 m/s during ebb, which corresponds to a Reynolds number of $\mathscr{O}(10^7)$. Although these are short datasets, they are sufficient to observe turbulent velocity fluctuations at a wide range of mean flow conditions at each site (e.g., 10 minute burst-averaged horizontal speeds varied from 0 to 2 m/s). Data are quality controlled to remove measurements with low beam correlations and low echo amplitude (less than 50 and less than 30 dB respectively for the Nortek Signature as per manufacturer recommendation). This excludes less than 0.5% of the raw data.

3. Analysis: Turbulent Kinetic Energy Dissipation Rate

At each depth in the ADCPs measured profiles, the TKE dissipation rate is estimated by two methodologies: from the frequency spectra (Lumley and Terray 1983) and from the spatial structure function (Wiles et al. 2006). Both methods are derived from Kolmorogv's turbulence hypotheses (Kolmogorov 1941; Pope 2001) and require the observation of the inertial subrange of isotropic turbulence.

a. Turbulent Kinetic Energy Spectra

The distribution of turbulent kinetic energy among eddies of different sizes is represented trough the turbulent kinetic energy spectra. Assuming stationarity, the turbulence advected past the instruments at average speeds $\bar{u}$ has frequency (f) spectra that are related to the wavenumber (k) spectra by $\bar{u} \propto f/k$ (i.e., Taylor's frozen field). Thus, the frequency spectra are expected to include an inertial sub-range, in which the turbulent kinetic energy follows $f^{-5/3}$ as a manifestation of the energy cascade following $k^{-5/3}$ (Kolmogorov 1941; Pope 2001).

TKE spectra are estimated using Welch's Overlapped Segment Averaging method applied to the vertical beam velocities (beam 5). For the Nortek Signature data sets, spectral estimates are calculated for every ten-minute burst using 23 50 s sub-windows with 50% overlap and a Hanning data taper, which results in an ensemble spectral density estimate with ~ 45 degrees of freedom. TKE spectra with the same degrees of freedom are also estimated for the RDI Sentinel V50 vertical beam velocities and for the Nortek Vector ADV measurements.

TKE spectra estimates for both sites for the tenth vertical bin (10.4 m from the sea bottom) are presented in Figure 3 colored by mean flow conditions. The TKE spectra estimates from the RDI Sentinel V50 measurements for the same bin are included in the Admiralty Inlet figures in grey. Averaged TKE spectra from the Nortek Vector ADV data is included for comparison as a red dashed line when available; the range of TKE spectra from the TTM ADV data is included as a pink area in the Admiralty Inlet plots. In this analysis, mean flows close to slack conditions ($\overline{u} < 0.5$ m/s) have been removed as the spectra does not show the theoretical $f^{-5/3}$ slope. Spectral density estimates from the Nortek Signature data are generally well sorted by mean flow velocity, implying that a higher TKE is observed at higher mean flows. The exception is during the stronger ebb at Rich Passage, where the instrument is in the lee of a sill.

The most novel result from the Nortek Signature data is the clear observation of the TKE energy cascade in the spectral estimates, which is usually obscured by the Doppler noise of profiling instruments. An isotropic region of tridimensional turbulence is present at mid frequencies ($0.1 < f < 1$ Hz) which follows the classic $f^{-5/3}$ energy cascade (Kolmogorov 1941). At higher ($f > 1$ Hz) frequencies, the spectra become affected by the instrument inherent Doppler noise. The spectral noise level of the Nortek Signature is observed around $S_w(f) = 10^{-4}$ m^{2}s^{-2}Hz^{-1}, while the noise level of the Nortek Vector is observed around $S_w(f) = 10^{-5}$ m^{2}s^{-2}Hz^{-1}. The noise level of the RDI Sentinel V50, by contrast, is much higher at $S_w(f) = 10^{-2}$ m^{2}s^{-2}Hz^{-1}, and thus the inertial subrange is obscured in those spectra.

The lower spectral noise floor observed from the Nortek Signature data can be attributed to its ability to sample faster. Even if the single-ping error is the same between the RDI Sentinel V50 and the Nortek Signature, the spectral noise floor will still be lower when the sampling is faster, as it is redistributed along a wider frequency range in the spectral energy density. In order to fairly compare the observed spectral noise floor of the two profilers, the data from the Nortek Signature is sub-sampled down to 2 Hz and new spectra are estimated (but not shown). For the sub-sampled case, the TKE energy cascade is still observed between $0.1 < f < 0.8$ Hz, and the noise level is observed around $S_w(f) = 2 * 10^{-4}$ m^{2}s^{-2}Hz^{-1}, which is slightly higher than when sampling at 8 Hz. The latter implies that even when sampling at the same frequency, the Nortek Signature presents a lower Doppler noise. The higher noise level prevents the use of the RDI Sentinel V50 data in the following estimation of TKE dissipation rate.

Figure 4 shows spectral estimates at maximum ebb and flood at the two sites for all vertical bins from the Nortek Signature data. The spectral estimates are well-sorted by depth, except for the maximum ebb at Rich Passage due to the existence of a vertical sill. TKE density decreases as the distance from the bottom increases, consistent with bottom-generated turbulence. In the higher bins, the observable portion of the inertial subrange becomes narrower due to the decrease in TKE density (noise floor affects spectra at a smaller frequency); for example at 20.4 m from the sea bottom the inertial subrange is observed at $0.1 < f < 0.6$ Hz.

The dissipation rate of TKE, ε, is related to the isotropic portion of the vertical TKE frequency spectrum by:

$$S_w(f) = \alpha \varepsilon^{2/3} f^{-5/3} \left(\frac{\bar{u}}{2\pi} \right)^{2/3} \tag{1}$$

where α is a constant equal to 0.69 (Sreenivasan 1995), ε is the TKE dissipation rate, f is the frequency and $\overline{u}$ is the mean along channel velocity. This applies Taylor's 'frozen field hypothesis ', which assumes that the turbulence is in steady state as it advects past the instrument (neither developing nor decaying), such that we can transform the temporal observation into a spatial one (i.e., $f = \overline{u}k/2\pi$, where k is the spatial wavenumber).

Each estimated spectra is multiplied by $f^{5/3}$ to obtain a compensated spectra, which is horizontal (flat) in the inertial subrange. The dissipation rate is estimated by solving $\overline{S_w(f)f^{5/3}|_{f_1}^{f_2}} = \alpha\varepsilon^{2/3}\left(\frac{\bar{u}}{2\pi}\right)^{2/3}$, where f_1 to f_2 is the frequency range with the slope closest to zero in the compensated spectra. The range of frequencies used to estimate the mean compensated spectra, $\overline{S_w(f)f^{5/3}}$, varies according to the position of the inertial subrange for different mean flows and depths, ranging between $0.1 < f < 1$ Hz. A minimum of five frequencies are used to estimate dissipation rates from the compensated spectra.

Uncertainties in the TKE dissipation rates from spectra are calculated by propagating the uncertainty in the compensated spectra (Bassett et al. 2013), such that:

$$e_{\varepsilon_S} = \frac{2\pi}{\overline{u}}\left(\frac{1}{\alpha}\right)^{3/2}\frac{3}{2}\overline{S_{w_{comp}}}^{1/2} e_{S_{w_{comp}}} \tag{2}$$

where e_{ε_S} is the uncertainty in the dissipation rate estimate, and $e_{S_{w_{comp}}}$ is taken to be the variance of the compensated spectra in the range of frequencies used to estimate ε.

b. Turbulence Structure Function

The along-beam velocities can be used to estimate the second-order spatial structure function of the along-beam turbulent fluctuations, $D(z,r)$, following the methodology described in Wiles et al. (2006). The structure function is defined as:

$$D_i(z,r) = \langle \left(u_i'(z+r) - u_i'(z)\right)^2 \rangle \tag{3}$$

where z is the along-beam measurement location, u_i' corresponds to each along-beam velocity fluctuation, and r is the distance between two velocity measurements; the angle brackets denote a time average over the burst.

The structure function $D_i(z,r)$ is estimated from the bottom of the profile upwards. The distance r is set to be positive and limited by the distance to the closest boundary, which in these cases is the sea bottom. Figure 5 shows examples of the spatial structure function for the vertical beam turbulent fluctuations, $D_5(z,r)$, at $z = 10.4$ m from the sea bottom at both sites. The structure function estimates from the RDI Sentinel V50 measurements for the same bin are included in the Admiralty Inlet figures in grey. Structure functions from the Nortek Signature data are generally well-sorted by the mean flow, except during the stronger ebb at Rich Passage, where again the sill creates a region of low turbulence. The slopes of the structure functions from the Nortek Signature agree well with the expected $r^{2/3}$ at both sites. Again, it is not possible to observe the theoretical $r^{2/3}$ slope in the structure function estimates from the RDI Sentinel V50. In these measurements the 1 m bin size, limits the turbulence length-scales observed, and particularly affects the observation of the inertial subrange on the turbulence structure function (McMillan and Hay 2017).

In the inertial subrange, the structure function is related to the distance r and to the dissipation rate ε by:

$$D_i(z,r) = C_v^2 \varepsilon^{2/3} r^{2/3} \tag{4}$$

where C_v^2 is a constant equal to 2.1 (Wiles et al. 2006; Thomson et al. 2012).

The structure function is multiplied by $r^{-2/3}$ to obtain a compensated structure function in the inertial subrange (Rusello and Cowen 2011). The dissipation rate is estimated by solving $\overline{D(z,r)r^{-2/3}\big|_{r_1}^{r_2}} = C_v^2 \varepsilon^{2/3}$, where r_1 to r_2 is the range with the slope closest to zero. Estimates are not calculated for depths with less than four points in the structure function. At Admiralty Inlet, the minimum r range used in the estimates is 1 to 4 m and the maximum range is 1 to 10 m; at Rich Passage the minimum range is 1 to 4 m, and the maximum range is 1 to 7 m. Within the valid depths, the structure function is quality controlled to remove estimates with negative slope, resulting in a loss of 21% of valid structure functions at Admiralty Inlet and 28% at Rich Passage, for which no dissipation estimate is available. Although this is a rather severe amount of quality control, it is less than that of other studies applying the structure function (McMillan et al. 2016; Thomson 2012).

Uncertainties in TKE dissipation rates from the structure function fitting are calculated by propagating the uncertainty in the compensated structure function, such that:

$$e_{\varepsilon_D} = \left(\frac{1}{Cv^2}\right)^{3/2} \frac{3}{2} \overline{D_{comp}}^{1/2} e_{D_{comp}} \tag{5}$$

were e_{ε_D} is the uncertainty in the dissipation rate estimate, and $e_{D_{comp}}$ is taken to be the variance of the compensated structure function in the range of bin separations used to estimate ε.

Figure 6 shows mean vertical profiles of TKE dissipation rates with their corresponding error estimates for both sites and compares the two methods. The dissipation rate estimates from the two methods are in agreement, although the estimates from the structure function do not cover the entire measured profile due to the r limitation. Estimates also are in good agreement with TKE dissipation rates estimated from ADV data spectral estimates, even at Rich Passage, where the TT ADV was located above the top of the profile measured by the Nortek Signature.

Summarized results of TKE dissipation rates from the two methods, and of the TKE dissipation rate uncertainty are presented in Table 2 for Admiralty Inlet and in Table 3 for Rich Passage.

4. Analysis: Turbulent Kinetic Energy Production Rate

In a well-mixed environment, the production from buoyancy can be neglected and the TKE is primarily produced by the mean flow shear. If horizontal shear is small, the TKE production can be approximated in terms of the Reynolds stresses and the velocity vertical gradients as:

$$P = -\overline{u'_{ch}w'}\frac{\partial \overline{u_{ch}}}{\partial z} - \overline{v'_{ch}w'}\frac{\partial \overline{v_{ch}}}{\partial z} - \overline{w'w'}\frac{\partial \overline{w}}{\partial z} \tag{6}$$

where P is the production of TKE, u_{ch}, v_{ch} and w are the along channel, across channel and vertical velocities respectively, and the primes denote velocity fluctuations.

a. Vertical Shear

Along-beam velocities are transformed into orthogonal east-north-up components. The horizontal components are rotated to obtain along and across channel velocity components at each location. The vertical gradients of the along channel, across channel and vertical velocity, $\frac{\partial \overline{u_{ch}}}{\partial z}$, $\frac{\partial \overline{v_{ch}}}{\partial z}$, $\frac{\partial \overline{w}}{\partial z}$, are estimated as the centered difference of their burst-average using the vertical distance between measurements.

The uncertainty in the shear estimations is calculated following Williams and Simpson (2004) method as:

$$e_S^2 = \frac{e_N^2}{M\Delta z^2 \sin^2 2\theta} \tag{7}$$

where e_N is the instrument inherent Doppler noise, M is the number of samples used in the burst-averaged and θ is the beam inclination angle. This estimate corresponds to the minimum level of shear detection considering only instrument noise as a source of error in the measurements (Williams and Simpson 2004). It has been previously reported that instrument noise from instrument softwares is usually biased low (Williams and Simpson 2004; Thomson et al. 2012). In this study, the instrument noise is estimated from the spectral noise level, as it is considered to be white noise (i.e. has a constant horizontal spectra) (McMillan and Hay 2017). The estimated instrument noise levels from spectra are: $e_N = 2.65$ cm/s for the Nortek Signature, and $e_N = 5.39$ cm/s for the RDI Sentinel V50. Instrument noise reported by the instruments corresponding software for each deployment and empirically estimated noise are shown in Table 1.

b. Reynolds Stresses

The Reynolds stress tensor is estimated following the methodology of Dewey and Stringer (2007) for a 5-beam ADCP configuration. This methodology extends the variance technique (Lu and Lueck 1999; Stacey et al. 1999; Rippeth et al. 2003) to different ADCP beam configurations including expressions for the Reynolds stresses for non-zero tilt. The use of five beams allows for exact expressions for five of the Reynolds stresses, total TKE and anisotropy (Dewey and Stringer 2007). This method assumes small angle approximations for pitch and roll, which were achieved in these deployments (mean pitch $\sim 2.3^\circ$ and mean roll $\sim 0.4^\circ$ at Admiralty Inlet, mean pitch $\sim 0.35^\circ$ and mean roll $\sim -1.19^\circ$ at Rich Passage). The Reynolds stresses from Dewey and Stringer (2007) are written in instrument coordinates (assuming heading is equal to zero), thus the obtained stresses are rotated to along and across channel coordinates after the calculations.

The following equations, from Dewey and Stringer (2007), define the Reynolds stresses in instruments coordinates for any 5-beam ADCP, assuming small tilt angles approximation:

$$
\begin{aligned}
\overline{u'^2} = \frac{-1}{4\sin^6\theta\cos^2\theta}\{&-2\sin^4\theta\cos^2\theta(\overline{u_2'^2}+\overline{u_1'^2}-2\cos^2\theta\overline{u_5'^2}) \\
&+2\sin^5\theta\cos\theta\phi_3(\overline{u_2'^2}-\overline{u_1'^2})\}
\end{aligned}
\tag{8}
$$

$$
\begin{aligned}
\overline{v'^2} = \frac{-1}{4\sin^6\theta\cos^2\theta}\{&-2\sin^4\theta\cos^2\theta(\overline{u_4'^2}+\overline{u_1'^3}-2\cos^2\theta\overline{u_5'^2})-2\sin^4\theta\cos^2\theta\phi_3(\overline{u_2'^2}-\overline{u_1'^2}) \\
&+2\sin^3\theta\cos^3\theta\phi_3(\overline{u_2'^2}-\overline{u_1'^2})-2\sin^5\theta\cos\theta\phi_2(\overline{u_4'^2}-\overline{u_3'^2})\}
\end{aligned}
\tag{9}
$$

$$
\begin{aligned}
\overline{w'^2} = \frac{-1}{4\sin^6\theta\cos^2\theta}\{&-2\sin^5\theta\cos\theta\phi_3(\overline{u_2'^2}-\overline{u_1'^2}+2\sin^5\theta\cos\theta\phi_2(\overline{u_4'^2}-\overline{u_3'^2}) \\
&-4\sin^6\theta\cos^2\theta\overline{u_5'^2})\}
\end{aligned}
\tag{10}
$$

$$
\begin{aligned}
\overline{u'w'} = \frac{-1}{4\sin^6\theta\cos^2\theta}\{&\sin^5\theta\cos\theta(\overline{u_2'^2}-\overline{u_1'^2})+2\sin^4\theta\cos^2\theta\phi_2(\overline{u_2'^2}+\overline{u_1'^2}) \\
&-4\sin^4\theta\cos^2\theta\phi_3\overline{u_5'^2}-4\sin^6\theta\cos^2\theta\phi_2\overline{u'v'}\}
\end{aligned}
\tag{11}
$$

$$
\begin{aligned}
\overline{v'w'} = \frac{-1}{4\sin^6\theta\cos^2\theta}\{&\sin^5\theta\cos\theta(\overline{u_4'^2}-\overline{u_3'^2})-2\sin^4\theta\cos^2\theta\phi_2(\overline{u_4'^2}+\overline{u_3'^2}) \\
&+4\sin^4\theta\cos^2\theta\phi_3\overline{u_5'^2}+4\sin^6\theta\cos^2\theta\phi_3\overline{u'v'}\}
\end{aligned}
\tag{12}
$$

where θ is the beam inclination angle (25° in these cases), ϕ_2 and ϕ_3 correspond to Dewey's pitch and roll respectively, and $\overline{u_i'^2}$ are the along-beam velocity fluctuation variances. For the Nortek Signature configuration: ϕ_2 corresponds to negative roll, and ϕ_3 to pitch, and $u_1 = u_{1Sig}$, $u_2 = u_{3Sig}$, $u_3 = u_{4Sig}$, and $u_4 = u_{2Sig}$. For the RDI Sentinel V50: ϕ_2 corresponds to roll, and ϕ_3 to pitch, and $u_1 = u_{2Sent}$, $u_2 = u_{1Sent}$, $u_3 = u_{4Sent}$, and $u_4 = u_{3Sent}$.

The Reynolds stress tensors are quality controlled to be a positive definite matrix. A total of 12% of the Reynolds stress tensors at Admiralty Inlet, and an 8% at Rich Passage, do not meet this requirement.

The uncertainty in the Reynolds stresses estimations is calculated following Williams and Simpson (2004) method as:

$$
e_{RS}^2 = \frac{e_N^4}{M\sin^2 2\theta}
\tag{13}
$$

where e_N is the instrument noise, M is the number of samples used in the averaging and θ is the beam inclination angle. This uncertainty estimate corresponds to the minimum level of Reynolds stress detection only considering instrument noise as for the estimation of shear uncertainty (Williams and Simpson 2004) .

A comparison between the obtained Reynolds stresses from the 5-beam profilers (after noise removal) and from direct covariance with the TTM ADV at Admiralty Inlet are shown in the scatter plot of Figure 7. Blue and red dots are averages binned by $\overline{u'_{ch}w'}$ from the TTM ADV measurements. Despite large scatter in the comparison, the binned results are in agreement at higher Reynolds stresses. The large differences might be explained by the separation of the instruments and by remaining noise in the Reynolds stress estimates.

Figures 8 and 9 show time series of vertical profiles of the five Reynolds stresses estimated following the Dewey and Stringer (2007) method at Admiralty Inlet and Rich Passage respectively. The horizontal Reynolds stresses ($\overline{u'^2_{ch}}$, $\overline{v'^2_{ch}}$) reach values that are an order of magnitude higher than the rest of the estimated Reynolds stresses at both sites. The magnitude of the Reynolds stresses are modulated by the tidal currents. At Admiralty Inlet, Reynolds stresses magnitudes increase as the horizontal speed increases, and the maximum values are observed during the observed ebb. At Rich Passage (Figure 9), the Reynolds stresses magnitude also increases with the horizontal speed. The highest Reynolds stresses are observed during the highest flood tidal current.

Figure 10 shows vertical profiles of the estimated vertical shear Reynolds stress ($\overline{u'_{ch}w'}$), averaged for ebb and flood at the two sites together with ADV estimates when available. Additionally, estimates using the variance technique with no tilt corrections for the two 5-beam Acoustic Doppler Current Profilers at both sites are included.

At Admiralty Inlet, during ebb, averaged estimates from the two instruments are in good agreement, and are also in good agreement with the TTM ADV estimates. For the first 15 m of the water column, the estimates from the Nortek Signature are higher than those from the RDI Sentinel V50. During flood, the RDI Sentinel V50 estimates are higher than those from the Nortek Signature through the entire water column. During ebb, the estimates from the variance technique are biased low during the lower portion of the water column and they are higher during the second portion of it. During flood, the variance technique estimates remain lower for most of the water column. This difference highlights the importance of the tilt corrections incorporated in the new calculations of the Reynolds stresses as previously reported by Lu and Lueck (1999).

At Rich Passage the two methods are in good agreement, with slightly lower estimates from the variance technique through the water column. However, the average estimate from the TT ADV at this site is much higher, which might be explained by motion contamination at low frequencies in u'_{ch} (Kilcher et al. In revision).

c. Vertical shear TKE Production

The estimated Reynolds stresses together with the vertical shear are used to estimate the vertical shear TKE production rate. The uncertainty in the TKE production estimations is calculated following Williams and Simpson (2004) method, which is based in the variance of the product of two variables:

$$e_{P_{ij}}^2 = \overline{u'_i u'_j}^2 e_S^2 + \frac{\partial \overline{u_i}}{\partial x_j} e_{RS}^2 + e_S^2 e_{RS}^2 \tag{14}$$

where $e_{P_{ij}}$ is the uncertainty associated with the TKE production generated by the Reynolds stress $\overline{u'_i u'_j}$ and the shear $\frac{\partial \overline{u_i}}{\partial x_j}$. Then the uncertainty of the vertical shear production P (Eq. 6) is estimated as:

$$e_P = \sqrt{e_{P_{u_{ch}w}}^2 + e_{P_{v_{ch}w}}^2 + e_{P_{ww}}^2} \tag{15}$$

Figure 12 shows averaged vertical profiles of TKE production for both sites separated by ebb and flood tides and their respective uncertainty. In these plots, the uncertainty in the production increases with z, because $e_{P_{\overline{ww}}}$, which is the dominating term in the production uncertainty, increases with z. The $e_{P_{\overline{ww}}}$ uncertainty is dominated by its first term, $\overline{w'w'}e_S^2$, which increases with z as would be expected as vertical fluctuations grow towards the mid water column, as the distance from the boundary increases.

Summaries of ebb and flood averages and standard deviations of TKE production rates, and their uncertainties are presented in Table 2 for Admiralty Inlet and in Table 3 for Rich Passage.

5. Application: Turbulent Kinetic Energy Balance

Assuming that the buoyancy term is negligible at these well-mixed sites and that self-advection is small, the rate of change of TKE can be approximated as a local production-dissipation balance,

$$\frac{D}{Dt}(TKE) \approx P - \varepsilon \tag{16}$$

Figure 11 shows the burst-averaged horizontal speed and vertical profiles in time of total TKE, TKE dissipation rate (from spectra), and TKE vertical production from the Nortek Signature data at both sites. At Admiralty Inlet, all three variables seem to be modulated by the stage of the tidal current, increasing as the velocity magnitude increases, however larger TKE, and TKE dissipation and production rates are observed during ebb. A similar pattern is observed at Rich Passage, where the variables are also modulated by the tidal currents, but larger values observed during the stronger flood.

Figure 12 shows an approximate TKE budget as depth profiles of vertical shear TKE production and TKE dissipation rates from the Nortek Signature data. Rates are averaged over all burst-average horizontal speeds, for ebb and flood at each site. The expected balance is generally found, however there are distinct patterns that likely are related to the lateral headland at Admiralty Inlet and the vertical sill at Rich Passage.

During ebb at Admiralty Inlet, TKE production exceeds dissipation close to the bottom and then an approximate balance is observed above $z = 10.4$ m. During flood, production and dissipation are approximately balance up to $z = 15.4$ m, and production exceeds dissipation in the higher portion of the water column. At Rich Passage, production is balanced by dissipation for most of the water column during ebb, except below $z = 5.4$ m, where dissipation exceeds production. During flood, dissipation exceeds production through the entire profile.

Figure 13 shows scatter plots of TKE production versus TKE dissipation rates for all burst-average velocities and all depths. The values are well correlated over several orders of magnitude, albeit with significant scatter. At Admiralty Inlet, a near 1:1 balance between TKE production and TKE dissipation during the most energetic conditions is observed. During less energetic conditions, TKE production exceeds TKE dissipation, suggesting that the transport of turbulent kinetic energy is of importance during such conditions. At Rich Passage, a near 1:1 balance between TKE production and TKE dissipation is observed during all conditions.

6. Conclusions

Two new 5-beam acoustic current profilers, the Nortek Signature 1000 (KHz) AD2CP and the RDI Sentinel V50 are successfully used to measure turbulence at two energetic tidal channels: Admiralty Inlet and Rich Passage (Puget Sound, WA, U.S.A). Turbulent kinetic energy (TKE) production and dissipation rates are estimated from the measurements, and an approximate TKE budget is obtained.

The results illustrate the capabilities of 5-beam profilers for assessing high order turbulence parameters. The TKE frequency spectra from the Nortek Signature presents a low noise level, of

$\mathscr{O}(10^{-4})$ m^{2}s^{-2}, while the RDI Sentinel V50 presents a higher noise level of $\mathscr{O}(10^{-2})$ m^{2}s^{-2} that is comparable to the previous generation of profilers.

The lower noise observed on the Nortek Signature spectra can be attributed to its ability to sample faster (8 Hz when using all 5 beams), however when subsampling the Nortek Signature data to 2 Hz (the maximum possible with the RDI), the noise level in the TKE spectra remains of $\mathscr{O}(10^{-4})$ m^{2}s^{-2}. The TKE spectra obtained with the Nortek Signature are in agreement with spectra from ADV measurements at both sites.

The lower noise level of the Nortek Signature enables observation of the inertial subrange of turbulence, and thus improved estimations of the TKE dissipation rate from both, TKE spectra and second order structure function of turbulence. TKE dissipation rates from the two methods agree well with each other through the water column, and also with estimates from ADV data.

Although the TKE spectra from the RDI Sentinel V50 does not allow the observation of the inertial subrange, the lower frequency portion of the spectra is well-resolved and in agreement with the estimates from the Nortek Signature and from the Nortek Vector. The RDI Sentinel V50 data can be used to estimate a synthetic vertical TKE spectra using the non-dimensional Kaimal curves (Kaimal et al. 1972). These curves can be fit to the lower portion of the TKE spectra and then used to extend the inertial subrange, and subsequently estimate the TKE dissipation rate. However, the derivation of the Kaimal curves is based on a balance between TKE production and dissipation, and might not be appropiate in the studied sites (Walter et al. 2011).

The use of all five beams enables the direct estimation of five out of six of the Reynolds stresses and thus improved estimations of the TKE production rate. The new Reynolds stresses calculations include tilt corrections following the Dewey and Stringer (2007) method. At Admiralty Inlet, Reynolds stresses estimates from the two profiling instruments are in agreement with estimates from ADV at higher Reynolds stresses .The differences might be attributed to instrument separation and to remaining noise in the Reynolds stresses estimations.

The obtained TKE dissipation rates and TKE production rates are used to analyze an approximate TKE budget at Admiralty Inlet and at Rich Passage. In general, the balance is observed, however, distinct patterns are observed at the two sites, which are thought to be related to bathymetric features that promote TKE advection and transport.

The turbulence parameters obtained with the new instruments are useful for the development of numerical models in these high flow environments, for the study of mixing processes, and for predicting sediment transport. The methods presented in this paper are implemented in Matlab and are available through the Matlab File Exchange website as 5-Beam Acoustic Doppler Current Profiler Turbulence Methods: `http://www.mathworks.com/matlabcentral/fileexchange/57551-mguerrap-5beam-turbulence-methods`

Acknowledgments. We thank Joe Talbert and Alex de Klerk for deployment and recovery of the instruments, and Andy Reay-Ellers for ship operations. We thank Levi Kilcher and Sam Harding for motion-corrected ADV data (used for validation). Funding was provided by NAVFAC. Maricarmen Guerra thanks the Fulbright and the Becas-Chile Conicyt doctorate fellowship programs.

References

Bassett, C., J. Thomson, and B. Polagye, 2013: Sediment-generated noise and bed stress in a tidal channel. *J. Geophys. Res. Oceans*, **118 (4)**, 2249–2265.

Brumley, B. H., R. G. Cabrera, K. L. Deines, and E. A. Terray, 1991: Performance of a broad-band acoustics Doppler current profiler. *J. Ocean. Eng.*, **16 (4)**.

Dewey, R., and S. Stringer, 2007: Reynolds stresses and turbulent kinetic energy estimates from various adcp beam configurations: Theory. *Unpublished*, 1–35.

Durgesh, V., J. Thomson, M. C. Richmond, and B. L. Polagye, 2014: Noise correction of turbulent spectra obtained from acoustic doppler velocimeters. *Flow Measurement and Instrumentation*, **37**, 29–41.

Harding, S., L. Kilcher, and J. Thomson, In revision: Turbulence measurements from compliant moorings - part i: motion characterization. *J. Atmos. Oceanic Technol.*

Kaimal, J., J. Wyngaard, Y. Izumi, and O. Coté, 1972: Spectral characteristics of surface-layer turbulence. *Q. J. R. Meteorol. Soc.*, **98 (417)**, 563–589.

Kilcher, L., S. Harding, J. Thomson, and S. Nylund, In revision: Turbulence measurements from compliant moorings - part i: motion correction. *J. Atmos. Oceanic Technol.*

Kolmogorov, A., 1941: Dissipation of energy in the locally isotropic turbulence. *Dokl. Akad. Nauk SSR*, **30**, 301–305.

Lu, Y., and R. Lueck, 1999: Using a broadband adcp in a tidal channel. part ii: Turbulence. *J. Atmos. Oceanic Technol*, **16 (11)**, 1568–1579.

Lumley, J. L., and E. A. Terray, 1983: Kinematics of turbulence convected by a random wave field. *J. Phys. Oceanogr.*, **13**, 2000–2007.

McMillan, J., and A. Hay, 2017: Spectral and structure function estimates of turbulence dissipation rates in a high-flow tidal channel using broadband adcps. *J. Atmos. Oceanic Technol*, **34 (1)**, 5–20.

McMillan, J., A. Hay, R. Lueck, and F. Wolk, 2016: Rates of dissipation of turbulent kinetic energy in a high reynolds number tidal channel. *J. Atmos. Oceanic Technol*, **33 (4)**, 817–837.

Pope, S. B., 2001: *Turbulent flows*. IOP Publishing.

Richard, J., J. Thomson, B. Polagye, and J. Bard, 2013: Method for identification of doppler noise levels in turbulent flow measurements dedicated to tidal energy. *Int. J. Marine Energy*, **3**, 52–64.

Rippeth, T., J. Simpson, E. Williams, and M. Inall, 2003: Measurement of the rates of production and dissipation of turbulent kinetic energy in an energetic tidal flow: Red wharf bay revisited. *J. Phys. Oceanogr.*, **33 (9)**, 1889–1901.

Rusello, P., and E. Cowen, 2011: Turbulent dissipation estimates from pulse coherent doppler instruments. *Proc. IEEE/OES 10th Current, Waves and Turbulence Measurements (CWTM), Monterey, CA.*, IEEE, 167–172.

Sreenivasan, K. R., 1995: On the universality of the kolmogorov constant. *Phys. Fluids*, **7 (11)**, 2778–2784.

Stacey, M., S. Monismith, and J. Burau, 1999: Measurements of reynolds stress profiles in unstratified tidal flow. *J. Geophys. Res.*, **104**, 10 935–10 949.

Thomson, J., 2012: Wave breaking dissipation observed with swift drifters. *J. Atmos. Oceanic Technol*, **29 (12)**, 1866–1882.

Thomson, J., B. Polagye, V. Durgesh, and M. Richmond, 2012: Measurements of turbulence at two tidal energy sites in Puget Sound, WA. *IEEE J. Oceanic Eng.*, **37 (3)**, 363–374.

Thomson, J., and Coauthors, 2013: Tidal turbulence spectra from a compliant mooring. *Proc. of the 1st Marine Energy Technical Symposium (METS), Washington D.C.*

Walter, R. K., N. J. Nidzieko, and S. G. Monismith, 2011: Similarity scaling of turbulence spectra and cospectra in a shallow tidal flow. *Journal of Geophysical Research: Oceans*, **116 (C10)**.

Wiles, P. J., T. P. Rippeth, J. H. Simpson, and P. J. Hendricks, 2006: A novel technique for measuring the rate of turbulent dissipation in the marine environment. *Geophys. Res. Lett.*, **33 (21)**.

Williams, E., and J. H. Simpson, 2004: Uncertainties in estimates of reynolds stress and tke production rate using the adcp variance method. *J. Atmos. Oceanic Technol*, **21 (2)**, 347–357.

LIST OF TABLES

TABLE 1. Summary of deployments and sampling parameters at Admiralty Inlet and Rich Passage.

Location	Admiralty Inlet	Admiralty Inlet	Admiralty Inlet	Rich Passage	Rich Passage
Instrument	Nortek Signature 1000	RDI Sentinel V50	Nortek Vector ADV	Nortek Signature 1000	Nortek Vector ADV
Latitude (°)	48.1522	48.1517	48.1524	47.5887	47.5887
Longitude (°)	-122.6852	-122.6858	-122.6868	-122.5641	-122.5641
Water Depth (m)	50	50	50	24	24
Deployment Duration (days)	2	2	2	2	0.1
Sampling Frequency (Hz)	8	2	16	8	16
Burst-Average (min)	10	10	10	10	10
Δz (m)	1	1	-	1	-
Distance to first cell (m)	0.5	0.5	-	0.5	-
Range (m)	20.5	20.5	-	15.5	-
z target (m)	-	-	10	-	17
Single ping error (m/s)	0.016	0.003	0.02	0.016	0.02
Empirical error (m/s)	0.027	0.054	0.011	0.027	0.011
Pitch °	2.26 ± 0.005	4.45 ± 0.06	-	0.35 ± 0.002	-
Roll °	0.36 ± 0.02	-1.61 ± 0.01	-	-1.19 ± 0.004	-

TABLE 2. Summary of ebb and flood averages ($\bar{x}$), standard deviations (σx), and averaged uncertainties ($\overline{e_x}$) of TKE dissipation and production rates at Admiralty Inlet. ε_{Sp} and ε_{SF} correspond to TKE dissipation rate estimated from TKE spectra and turbulence structure function respectively, P corresponds to TKE production.

		Ebb			Flood		
z (m)	ε, P (m^2s^{-3})	$\bar{x}$	σ_x	$\overline{e_x}$	$\bar{x}$	σ_x	$\overline{e_x}$
5.4	ε_{Sp}	6.54E-05	5.42E-05	1.00E-05	8.30334E-05	6.77E-05	1.37E-05
	ε_{SF}	3.86E-05	2.32E-05	5.91E-06	4.09142E-05	2.38E-05	5.24558E-06
	P	1.13E-04	9.71E-05	7.02E-06	7.75989E-05	6.35E-05	6.72E-06
10.4	ε_{Sp}	3.73E-05	3.79E-05	5.45E-06	2.49E-05	2.46E-05	4.50E-06
	ε_{SF}	3.33E-05	2.20E-05	5.15E-06	2.41E-05	1.44E-05	3.53E-06
	P	2.59E-05	2.65E-05	6.18E-06	2.69E-05	2.81E-05	5.28E-06
15.4	ε_{Sp}	1.74E-05	1.85E-05	4.34E-06	1.31E-05	1.69E-05	2.39E-06
	ε_{SF}	2.43E-05	1.95E-05	5.79E-06	1.70E-05	1.16E-05	3.11E-06
	P	1.79E-05	2.23E-05	8.00E-06	2.98E-05	3.04E-05	5.39E-06
19.4	ε_{Sp}	1.39E-05	2.70E-05	2.44E-06	1.00E-05	1.33E-05	1.89E-06
	ε_{SF}	-	-	-	-	-	-
	P	9.78E-06	1.18E-05	1.05E-05	2.41E-05	2.55E-05	4.77E-06

TABLE 3. Summary of ebb and flood averages ($\bar{x}$), standard deviations (σx), and averaged uncertainties ($\overline{e_x}$) of TKE dissipation and production rates at Rich Passage. ε_{Sp} and ε_{SF} correspond to TKE dissipation rate estimated from TKE spectra and turbulence structure function respectively, P corresponds to TKE production.

		Ebb			Flood		
z (m)	ε, P (m^{2}s^{-3})	$\bar{x}$	σ_x	$\overline{e_x}$	$\bar{x}$	σ_x	$\overline{e_x}$
5.4	ε_{Sp}	9.87E-06	9.50E-06	2.03E-06	4.89E-05	5.68E-05	8.86E-06
	ε_{SF}	1.05E-05	5.60E-06	1.20E-06	3.33E-05	3.03E-05	4.43E-06
	P	8.08E-06	8.11E-06	2.50E-06	2.12E-05	1.90E-05	5.41E-06
10.4	ε_{Sp}	4.02E-06	6.71E-06	1.02E-06	1.46E-05	2.34E-05	2.66E-06
	ε_{SF}	7.93E-06	4.27E-06	8.59E-07	1.46E-05	1.09E-05	1.72E-06
	P	3.87E-06	4.27E-06	2.21E-06	7.79E-06	1.03E-05	3.33E-06
14.4	ε_{Sp}	3.17E-06	3.49E-06	6.71E-07	5.52E-06	1.02E-05	1.31E-06
	ε_{SF}	-	-	-	-	-	-
	P	4.66E-06	6.72E-06	2.52E-06	3.43E-06	4.72E-06	2.32E-06

LIST OF FIGURES

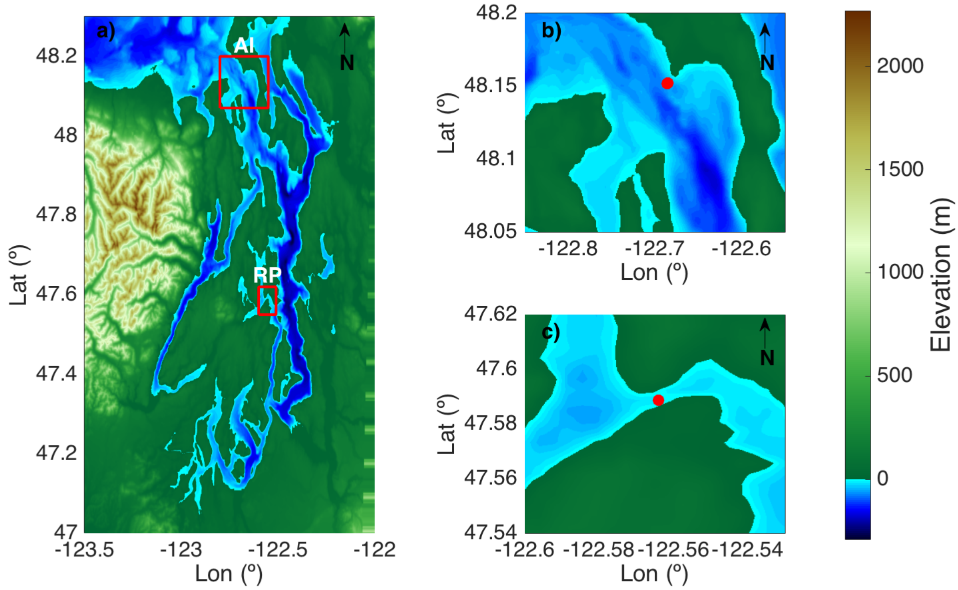

561 FIG. 1. Bathymetry and location of the two tidal channels: a) Puget Sound in Washington, U.S.A., b) Admiralty Inlet (AI) and c) Rich Passage (RP). Red dots indicate instruments location.

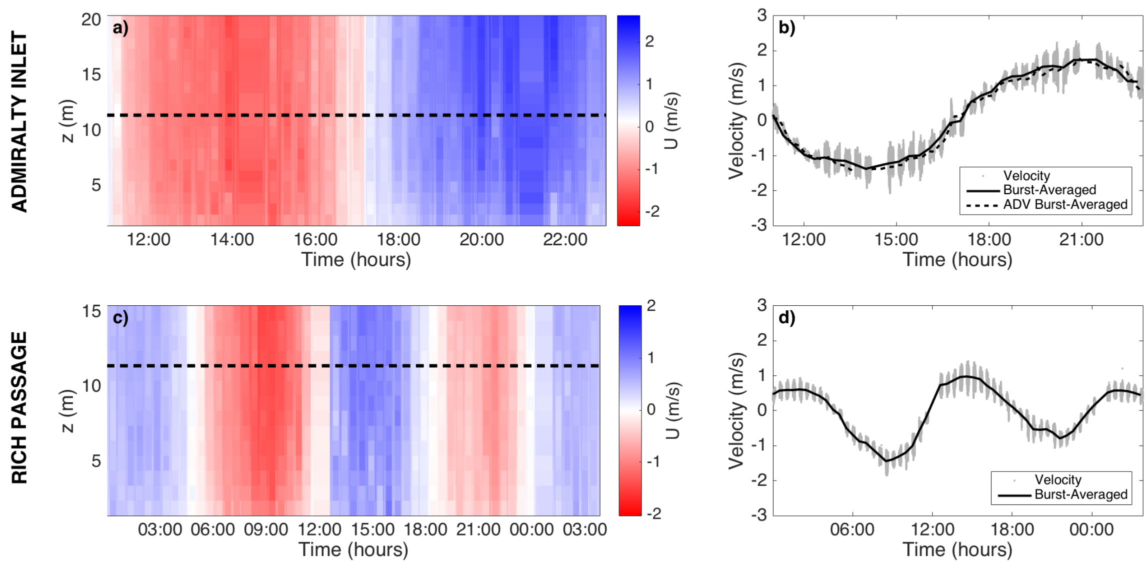

FIG. 2. Vertical profiles and time series of along-channel velocities measured with the Nortek Signature: a), b) at Admiralty Inlet, and c), d) at Rich Passage. In a) and c) black dashed line indicates depth corresponding to the time series (as $z = 10.4$ m from sea-bottom). In b) and d), grey dots correspond to measured along-channel velocity, and black line corresponds to 10 minute burst-averaged along-channel velocity. Burst-averaged along-channel velocity measured with the TTM ADV at Admiralty Inlet is included as a black dashed line in b).

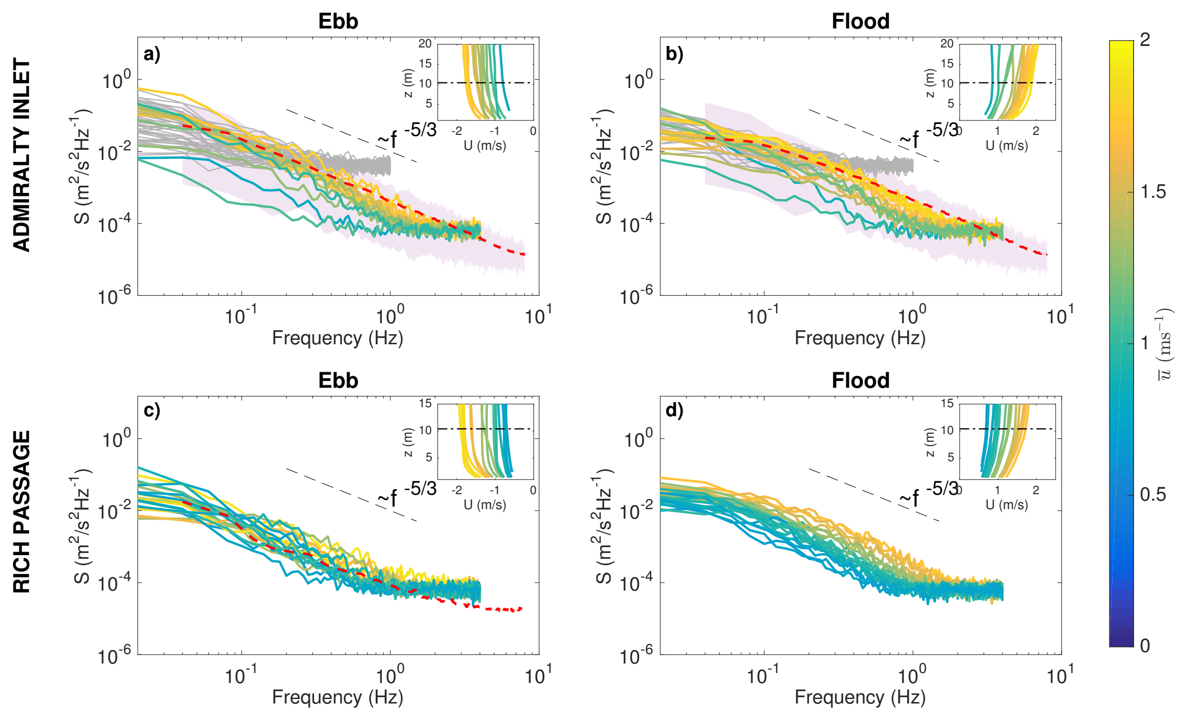

FIG. 3. TKE spectra at $z = 10.4$ m for different mean flows (by color): a), b) at Admiralty Inlet, and c), d) at Rich Passage. Dashed black line is proportional to $f^{-5/3}$. Inset plots show burst-average horizontal speed vertical profiles (also by color); dot-dashed line shows $z = 10.4$ m in the profiles. In the Admiralty Inlet plots, spectra from the RDI Sentinel V50 data are included as grey curves, and the range of spectra from the TTM ADV data is included as a light pink are. Dashed line corresponds to averaged spectra from ADV data.

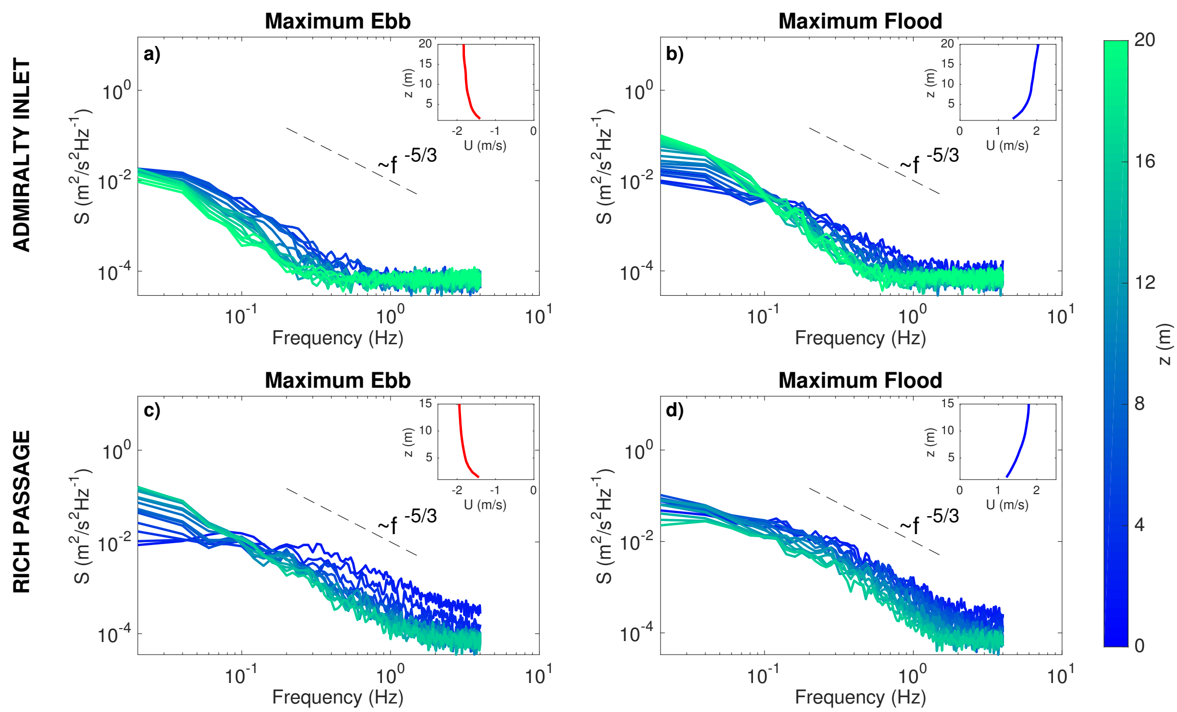

FIG. 4. TKE spectra at maximum ebb and flood mean flow conditions at different depths (by color): a), b) at Admiralty Inlet, and c), d) at Rich Passage. Dashed black line is proportional to $f^{-5/3}$. Inset plots show corresponding mean flow vertical profile.

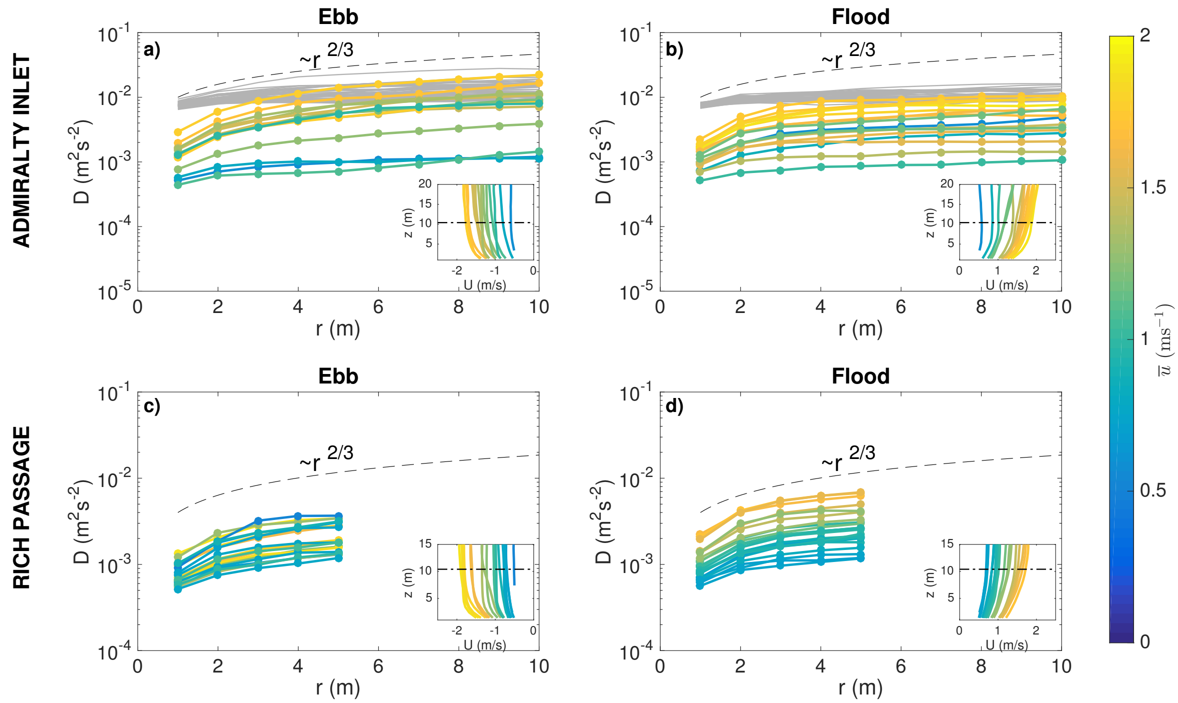

FIG. 5. Spatial structure function at $z = 10.4$ m for different mean flows (by color): a), b) at Admiralty Inlet, and c), d) at Rich Passage. The dashed line is proportional to $r^{2/3}$. Inset plots show mean flow vertical profiles (also by color); the dot-dashed line corresponds to $z = 10.4$ m. In the Admiralty Inlet plots, structure functions from the RDI Sentinel V50 data are included as grey curves.

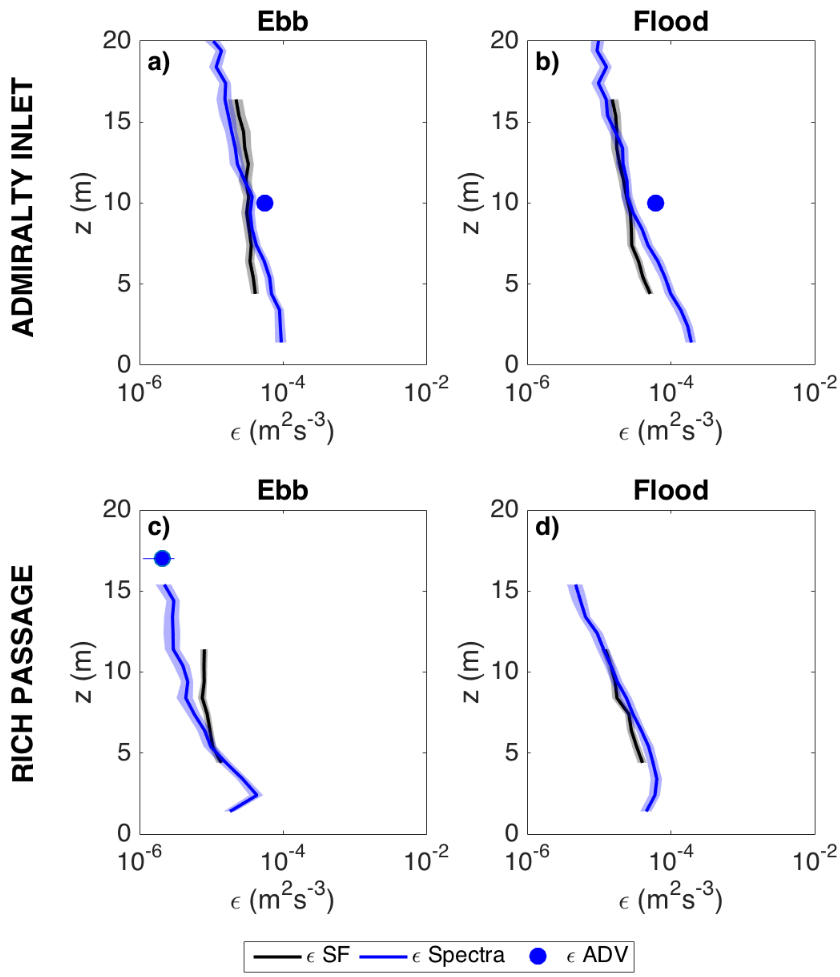

FIG. 6. Average vertical profiles of TKE dissipation rate at: a), b) at Admiralty Inlet, and c), d) at Rich Passage. In blue from the TKE spectra and in black from the turbulence structure function. Blue dots correspond to TKE dissipation rate estimates from the TTM ADV spectra.

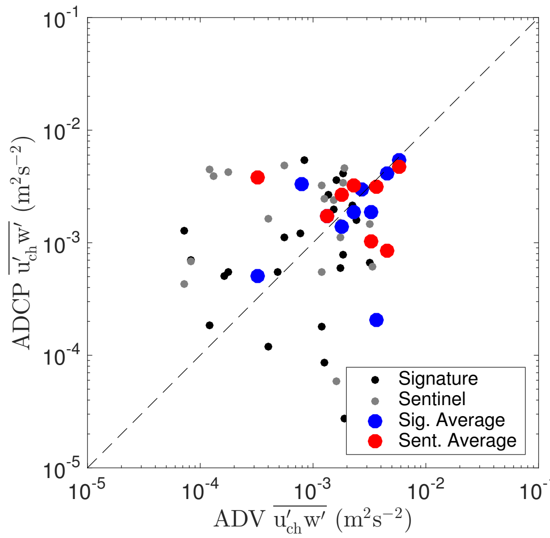

FIG. 7. Vertical shear Reynolds stress ($\overline{u'_{ch}w'}$) at Admiralty Inlet: from TTM ADV data (x-axis), and from Nortek Signature and RDI Sentinel V50 estimated using Dewey and Stringer (2007) 5-beam method (y-axis). Blue and red dots are averages binned by $\overline{u'_{ch}w'}$ from the TTM ADV measurements. Black-dashed line correspond to $y = x$. Averaged data correlation coefficients: 0.6 (Nortek Signature to TTM ADV), 0.05 (RDI Sentinel V50 to TTM ADV).

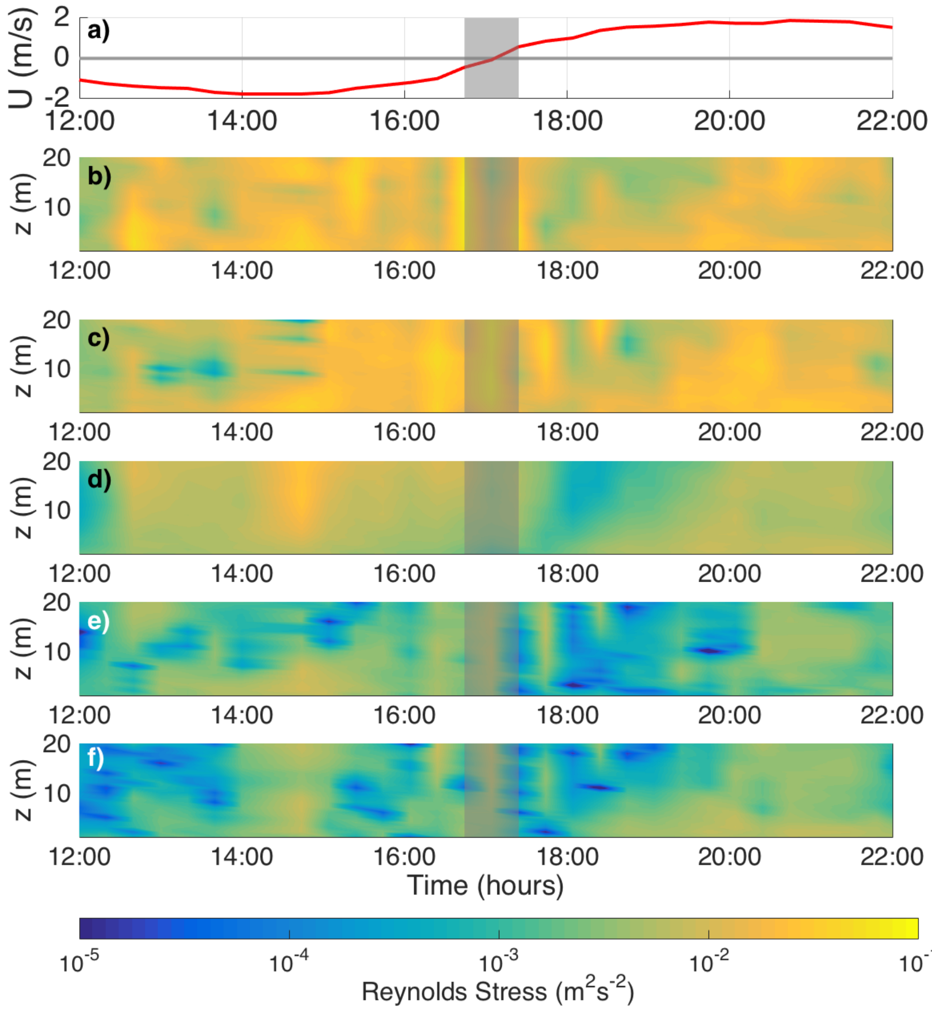

FIG. 8. Horizontal burst-averaged speed and vertical profiles of Reynolds stresses in time estimated using Dewey and Stringer (2007) 5-beam method at Admiralty Inlet: a) Mean flow, b) $\overline{u'^2_{ch}}$, c) $\overline{v'^2_{ch}}$, d) $\overline{w'^2}$, e) $\overline{u'_{ch}w'}$, and f) $\overline{v'_{ch}w'}$. Slack conditions are marked in grey.

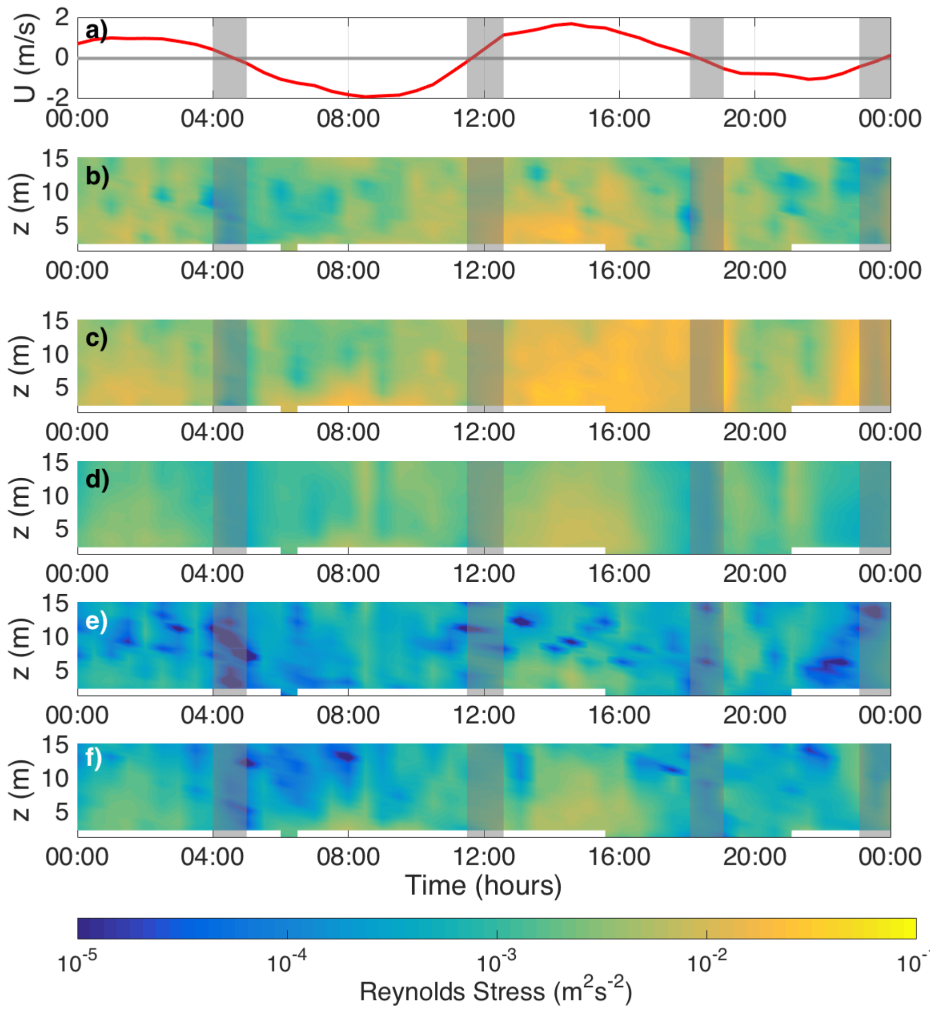

591 FIG. 9. Horizontal burst-averaged speed and vertical profiles of Reynolds stresses in time estimated using
592 Dewey and Stringer (2007) 5-beam method at Rich Passage: a) Mean flow, b) $\overline{u'^2_{ch}}$, c) $\overline{v'^2_{ch}}$, d) $\overline{w'^2}$, e) $\overline{u'_{ch}w'}$, and
593 f) $\overline{v'_{ch}w'}$. Slack conditions are marked in grey.

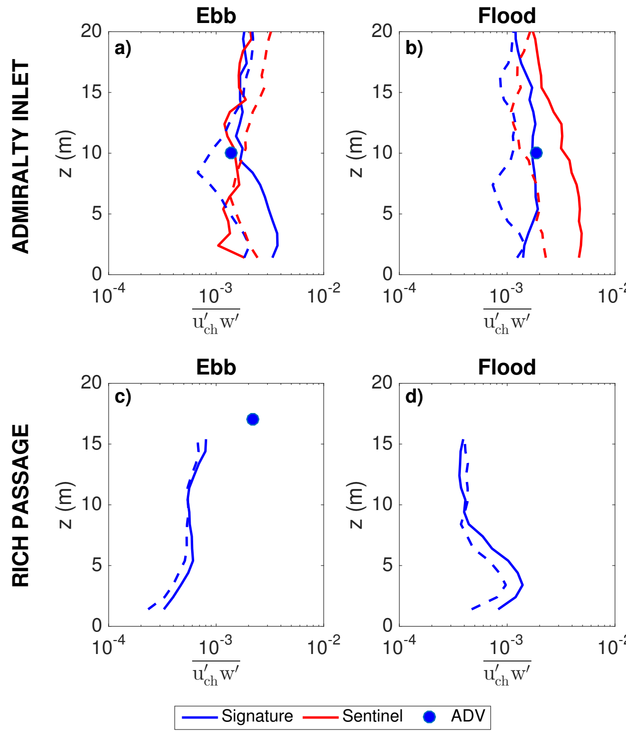

FIG. 10. Average vertical shear Reynolds stress ($\overline{u'_{ch}w'}$) profiles estimated using Dewey and Stringer (2007) 5-beam method at: a), b) at Admiralty Inlet, and c), d) at Rich Passage. In blue from the Nortek Signature data, in red from the RDI Sentinel V50 data. Dashed lines correspond to estimates using the original variance technique with no tilt corrections (Stacey et al. 1999). Blue dots correspond to estimates from the ADV data.

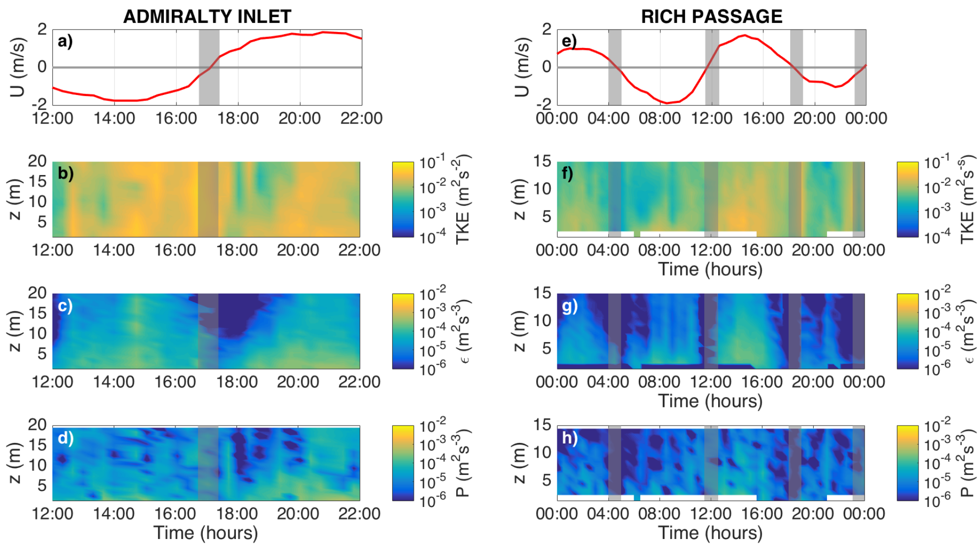

FIG. 11. Vertical profiles of TKE dissipation and production rates in time at Admiralty Inlet (left) and at Rich Passage (right). Panels show: a) and e) Mean horizontal speed, b) and f) Total TKE, c) and g) TKE dissipation rate, d) and h) TKE production rate.

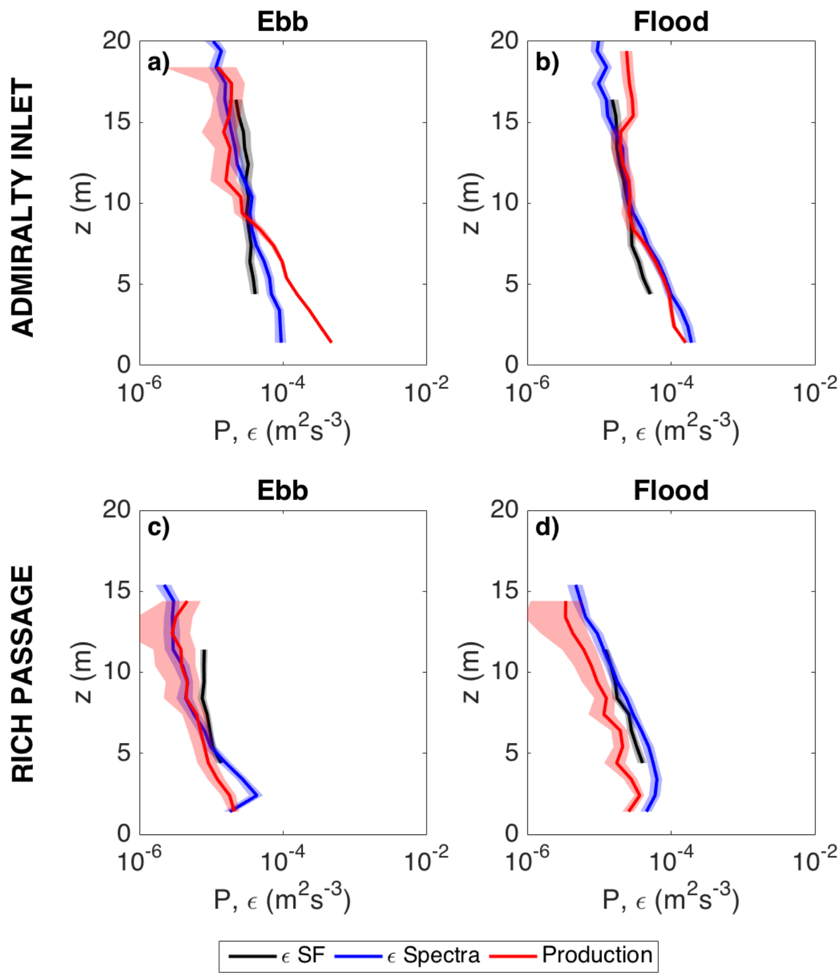

601 FIG. 12. An approximate TKE budget shown using average TKE dissipation rates from the two methods and
602 TKE shear production from Reynolds stresses from the Nortek Signature data: a), b) at Admiralty Inlet, and c),
603 d) at Rich Passage.

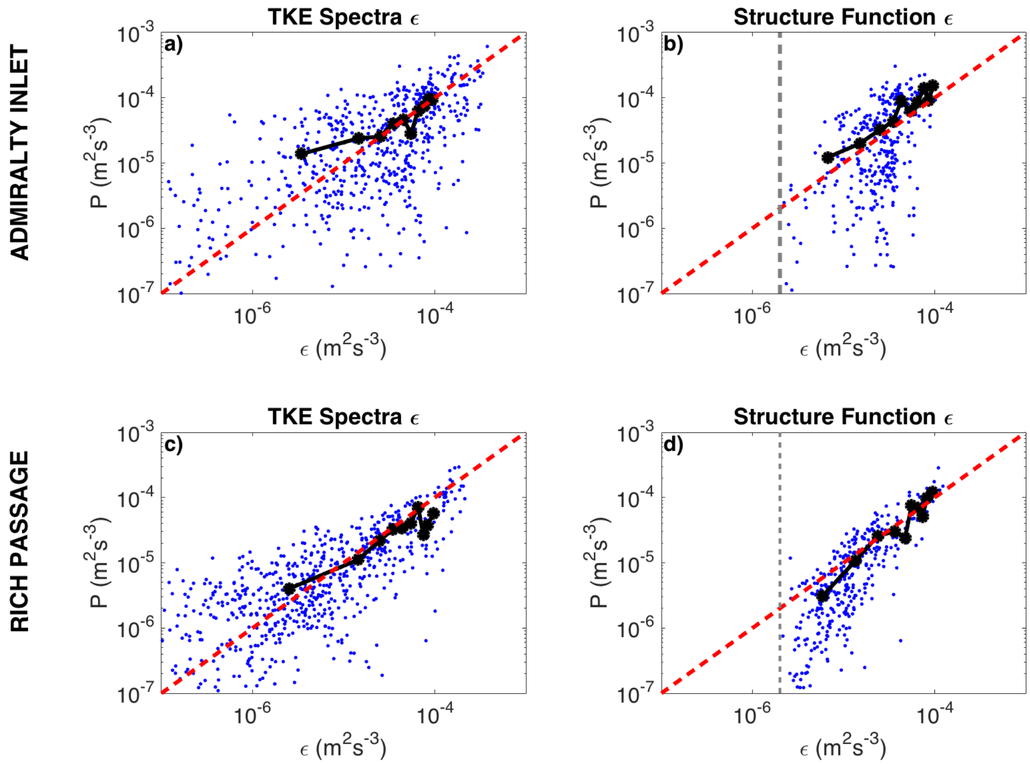

FIG. 13. TKE Dissipation Rate and TKE Production for all $\bar{u}$ and all depths: a), b) at Admiralty Inlet and b), c) at Rich Passage. Black dots represent mean values of dissipation and production binned by dissipation. Red dashed line corresponds to $y = x$. In the plots showing the TKE dissipation rate from the structure function, the dashed grey line represents the limit of TKE dissipation detection when using the turbulence structure function.